PRAMANA — journal of physics

Vol. 76, No. 1
January 2011
pp. 127–138

Atomistic simulation of the point defects in TaW ordered alloy

ZHONG-LIANG LIN[1], JIAN-MIN ZHANG[1,*], YAN ZHANG[2] and VINCENT JI[2]
[1]College of Physics and Information Technology, Shaanxi Normal University, Xian 710062, Shaanxi, People's Republic of China
[2]ICMMO/LEMHE UMR CNRS 8182, Université Paris-Sud 11, 91405 Orsay Cedex, France
*Corresponding author. E-mail: jianm_zhang@yahoo.com

MS received 12 June 2010; accepted 14 July 2010

Abstract. Combining molecular dynamics (MD) simulation with modified analytic embedded-atom method (MAEAM), the formation, migration and activation energies of the point defects for six-kind migration mechanisms in B_2-type TaW alloy have been investigated. The results showed that the anti-site defects Ta_W and W_{Ta} were easier to form than Ta and W vacancies owing to their lower formation energies. Comparing the migration and activation energies needed for six-kind migration mechanisms of a Ta (or W) vacancy, we found that one nearest-neighbour jump (1NNJ) was the most favourable because of its lowest migration and activation energies, but it would lead to a disorder in the alloy. One next-nearest-neighbour jump (1NNNJ) and one third-nearest-neighbour jump (1TNNJ) could maintain the ordered property of the alloy but required higher migration and activation energies. So the 1NNNJ and 1TNNJ should be replaced by straight [100] six nearest-neighbor cyclic jumps (S[100]6NNCJ) (especially) or bent [100] six nearest-neighbour cyclic jumps (B[100]6NNCJ) and [110] six nearest-neighbor cyclic jumps ([110]6NNCJ), respectively.

Keywords. TaW alloy; vacancy; anti-site defect; migration mechanism; modified analytic embedded-atom method.

PACS Nos 61.82.Bg; 61.72.Bb; 66.30.Fq

1. Introduction

TaW alloy is widely used as a high-temperature technological material in the industry due to its excellent strength at elevated temperature and therefore it is found useful for high-temperature aerospace and nuclear applications. It is well known that the point defects play an important role in the processes of diffusion [1], oxidation [2], crystal growth [3], and all these directly affect the kinetic and thermodynamic behaviours of the alloys. This fact has led us to get a good understanding of their formation and migration mechanisms in the alloys. Although first-principles calculations based on density functional theory

[4] are now routinely used to predict the structural [5,6], magnetic [7,8], electrical [9,10] and optical [11] properties of a wide range of materials [12], thermodynamic properties of the alloys are still beyond the reach of the first-principles calculations, as they require very big simulation cells and long simulation time [13]. To overcome these limitations, the formation and migration mechanisms of the point defects (vacancy and anti-site defect) in B_2-type TaW alloy [14] have been investigated by combining molecular dynamics (MD) simulation with modified analytic embedded-atom method (MAEAM) [15–17]. In our previous papers, the MAEAM was used successfully to calculate the phonon dispersion for body-centred cubic alkali metals [18], grain boundary energy [19], mechanical stability and strength [20], the formation and migration energy of an isolated vacancy and adatom in three noble metals [21], the self-diffusion of BCC transition metals [22] and the properties of the intermetallic compound [23].

The following are discussed in this paper. (1) The lattice constant and formation energy of the B_2-type TaW alloy were calculated from the energy minimization. The results are in good agreement with the *ab initio* data [13]. (2) The formation energies of the Ta and W vacancies V_{Ta} and V_W, and anti-site defects Ta_W (Ta occupies W sublattice) and W_{Ta} (W occupies Ta sublattice) were calculated. Both anti-site defects Ta_W and W_{Ta} (especially) are favourable defects because of their lower formation energies. (3) The migration and activation energies have also been determined from energy displacement curves for the Ta and W vacancies V_{Ta} and V_W, using the following six migration mechanisms: (a) one nearest-neighbour jump (1NNJ), (b) one next-nearest-neighbour jump (1NNNJ), (c) one third-nearest-neighbour jump (1TNNJ), (d) bent [100] six nearest-neighbour cyclic jumps (B[100]6NNCJ), (e) straight [100] six nearest-neighbour cyclic jumps (S[100]6NNCJ) and (f) [100] six nearest-neighbour cyclic jumps ([110]6NNCJ). The 1NNJ is the most favourable because of its lowest migration and activation energies, but it will lead to a disorder in the alloy. Both the 1NNNJ and 1TNNJ, especially the 1TNNJ, can maintain the ordered property of the alloy, but require higher migration and activation energies. So the 1NNNJ and 1TNNJ should be replaced by S[100]6NNCJ (especially) or B[100]6NNCJ, and [110]6NNCJ, respectively.

2. Computation methodology and procedure

2.1 *MAEAM*

In MAEAM, the total energy E_t of a crystal is expressed as [17]

$$E_t = \sum_i F(\rho_i) + \frac{1}{2}\sum_i \sum_{j\neq i} \phi(r_{ij}) + \sum_i M(P_i), \tag{1}$$

$$\rho_i = \sum_{j\neq i} f(r_{ij}), \tag{2}$$

$$P_i = \sum_{j\neq i} f^2(r_{ij}), \tag{3}$$

where $F(\rho_i)$ is the energy to embed an atom in site i with electron density ρ_i, which is given by a linear superposition of the spherical averaged atomic electron density of

other atoms $f(r_{ij})$, r_{ij} is the separation distance of atom j from atom i, $\phi(r_{ij})$ is the pair potential between atoms i and j, and $M(P_i)$ is the modified term, which describes the energy deviation from the linear superposition. Embedding function $F(\rho_i)$, pair potential $\phi(r_{ij})$, modified term $M(P_i)$ and atomic electron density $f(r_{ij})$ take the following forms [15,17]:

$$F(\rho_i) = -F_0 \left[1 - n \ln\left(\frac{\rho_i}{\rho_e}\right)\right] \left(\frac{\rho_i}{\rho_e}\right)^n, \tag{4}$$

$$\phi(r_{ij}) = k_0 + k_1 \left(\frac{r_{ij}}{r_{1e}}\right)^2 + k_2 \left(\frac{r_{ij}}{r_{1e}}\right)^4 + k_3 \left(\frac{r_{1e}}{r_{ij}}\right)^{12}, \quad r_{ij} \le r_{2e}, \tag{5}$$

$$\begin{aligned}\phi(r_{ij}) = {} & l_0 + l_1 \left(\frac{r_{ij}}{r_{2e}} - 1\right) + l_2 \left(\frac{r_{ij}}{r_{2e}} - 1\right)^2 \\ & + l_3 \left(\frac{r_{ij}}{r_{2e}} - 1\right)^3, \quad r_{2e} < r_{ij} \le r_c,\end{aligned} \tag{6}$$

$$M(P_i) = \alpha \left(\frac{P_i}{P_e} - 1\right)^2 \exp\left[-\left(\frac{P_i}{P_e} - 1\right)^2\right], \tag{7}$$

$$f(r_{ij}) = f_e \left(\frac{r_{1e}}{r_{ij}}\right)^6, \tag{8}$$

where the subscript e denotes equilibrium state, $r_c = r_{2e} + 0.75(r_{3e} - r_{2e})$ is the cut-off distance and r_{1e}, r_{2e} and r_{3e} are the first, second and third nearest-neighbour distances at equilibrium. In this paper, the atomic electron density at equilibrium state f_e is chosen as $f_e = E_c/V$ [24], where $V = a^3/2$ is the atomic volume for a metal with BCC structure.

The parameters F_0, n, a, k_i and l_i ($i = 0, 1, 2, 3$) in eqs (4)–(7) can be determined by fitting the lattice constant a, cohesion energy E_c, vacancy formation energy E_v^f and elastic constants C_{11}, C_{12} and C_{44}. The physical parameters and the calculated model parameters for Ta and W are listed in tables 1 and 2, respectively.

For the B_2-type TaW ordered alloy, the Ta–Ta and W–W interaction potentials can be described by eqs (5) and (6) in MAEAM, whereas for Ta–W interactions, we take Johnson's formula [26]

$$\phi^{\mathrm{Ta-W}}(r_{ij}) = \frac{1}{2}\left[\frac{f^{\mathrm{Ta}}(r_{ij})}{f^{\mathrm{W}}(r_{ij})}\phi^{\mathrm{W}}(r_{ij}) + \frac{f^{\mathrm{W}}(r_{ij})}{f^{\mathrm{Ta}}(r_{ij})}\phi^{\mathrm{Ta}}(r_{ij})\right], \tag{9}$$

where the superscripts Ta, W in the electron density function $f(r_{ij})$ and interaction potential $\phi(r_{ij})$ represent them for Ta and W, respectively.

By substituting the parameters listed in table 2 into eqs (5), (6) and (9), the pair potentials for Ta–Ta, W–W and Ta–W are determined and are shown in figure 1. The variation of the average energy per atom in perfect TaW alloy system with lattice constant is shown

Table 1. The input physical parameters of Ta and W [25].

Elements	a (Å)	E_{c} (eV)	E_v^f (eV)	C_{11} (eV/Å^3)	C_{12} (eV/Å^3)	C_{44} (eV/Å^3)
Ta	3.3026	8.10	2.95	1.64	0.97	0.52
W	3.1650	8.90	3.95	3.23	1.27	0.98

Table 2. The MAEAM model parameters for Ta and W.

Elements	n	a	F_0 (eV)	k_0 (eV)	k_1 (eV)	k_2 (eV)	k_3 (eV)	l_0 (eV)	l_1 (eV)	l_2 (eV)	l_3 (eV)
Ta	0.3611	0.1693	5.15	0.0166	−1.1950	0.6498	0.0945	−0.4046	1.2326	4.6417	−14.218
W	0.4630	0.0110	4.95	1.5004	−4.1373	1.9416	0.1156	−0.5437	2.5272	0.6311	−10.083

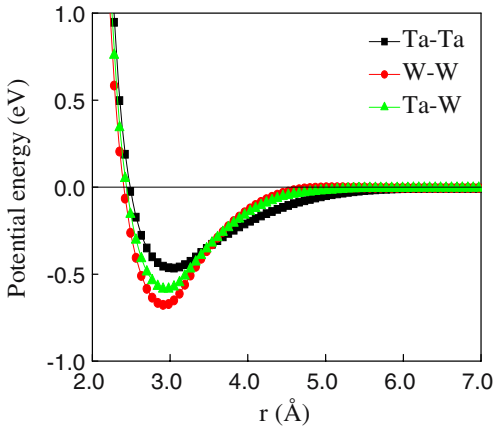

Figure 1. The pair potentials of Ta–Ta, W–W and Ta–W.

in figure 2, in which, the abscissa and ordinate values at the vale point correspond to the equilibrium lattice constant a and cohesion energy E_c of a perfect TaW alloy system, respectively.

2.2 *The configurations of the defects in B_2-type TaW ordered alloy*

In a perfect B_2-type TaW ordered alloy, as shown in figure 3a, the Ta atoms (gray balls) are located on the vertices of a unit cell and the W atoms (black squares) are arranged at the centre and vice versa. Both the vacancy and anti-site defect are considered in this paper.

(1) Vacancy (figure 3b), the absence of a Ta or a W atom on Ta or W sublattice site forms a Ta vacancy V_{Ta} or a W vacancy V_W. (2) Anti-site defect (figure 3c), a Ta atom replaces a W atom or a W atom replaces a Ta atom and forms a Ta anti-site defect Ta_W or a W anti-site defect W_{Ta}.

2.3 *Calculation procedure*

The molecular dynamics simulation is conducted in an $8a \times 8a \times 8a$ computational cell, where *a* is the lattice constant of the alloy. One of the point defects is created in the centre of the cell and the total energy is minimized with respect to local atomic displacements with a simultaneous volume relaxation. The formation energies of the vacancy, anti-site defect and the alloy are calculated by the following formulas:

$$E^f_{1v}(A) = E_{\rm rel}(n-1) - E_{\rm per}(n) + E_c(A), \tag{10}$$

$$E^f_{\rm ant}(A_B) = E_{\rm rel}(n) - E_{\rm per}(n) + E_c(B) - E_c(A), \tag{11}$$

$$\Delta E_c = E_{\rm per}(n)/n - xE'_c({\rm Ta}) - (1-x)E'_c({\rm W}), \tag{12}$$

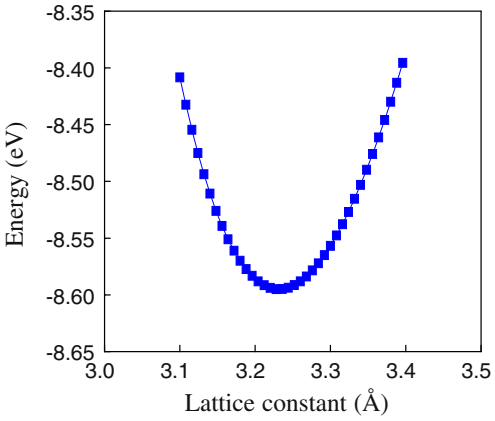

Figure 2. Energy per atom vs. lattice constant for the TaW alloy.

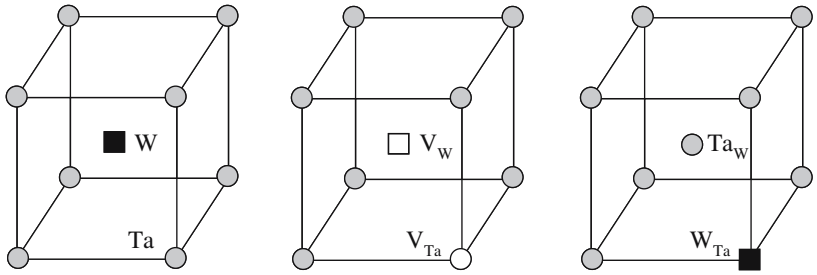

Figure 3. Unit cell of TaW ordered alloy with and without point defect: (**a**) perfect lattice, (**b**) vacancy and (**c**) anti-site defect.

where the parameters A or B represents the element Ta or W in the alloy, x is the atomic proportion of the Ta elements in the alloy (here, $x = 0.5$ for B_2-type TaW-ordered alloy), $E_{\mathrm{rel}}(n-s)(s=0,1)$ and $E_{\mathrm{per}}(n)$ represent the total energy of the system with and without defect, respectively, $E_{\mathrm{c}}(A)$ or $E_{\mathrm{c}}(B)$ is the cohesion energy of the element Ta or W in the alloy, and $E'_{\mathrm{c}}(\mathrm{Ta})$ or $E'_{\mathrm{c}}(\mathrm{W})$ is the cohesion energy of a pure Ta or W metal.

Taking the migration of a Ta vacancy V_{Ta} in TaW alloy as an example, one nearest-neighbour jump (1NNJ) is shown in figure 4a, one next-nearest-neighbour jump (1NNNJ) is shown in figure 4b, one third-nearest-neighbour jump in figure 4c (1TNNJ), bent [100] six nearest-neighbour cyclic jumps (B[100]6NNCJ) are shown in figure 4d, straight [100] six nearest-neighbour cyclic jumps (S[100]6NNCJ) is shown in figure 4e and [110] six nearest-neighbour cyclic jumps ([110]6NNCJ) are shown in figure 4f. The migration mechanisms (d) B[100]6NNCJ and (e) S[100]6NNCJ are considered here for comparing

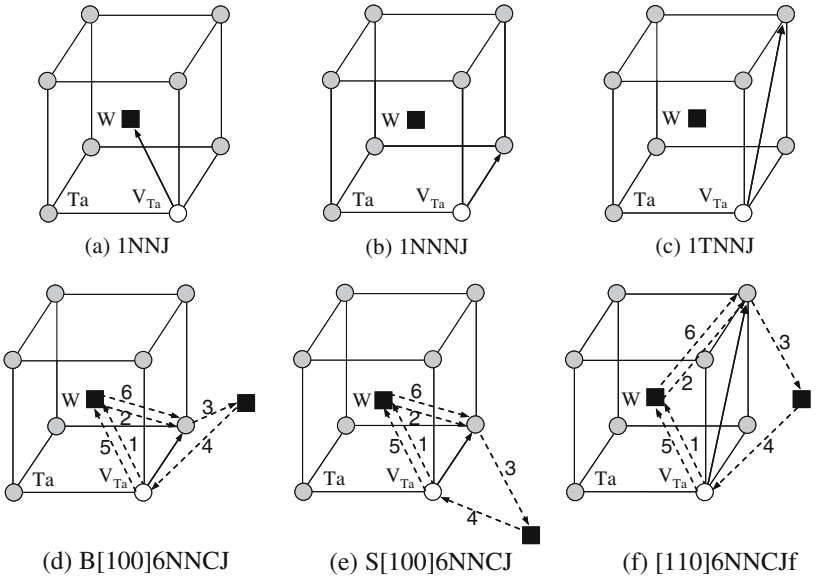

Figure 4. The six migration mechanisms of Ta vacancy V_{Ta}: (**a**) 1NNJ, (**b**) 1NNNJ, (**c**) 1TNNJ, (**d**) B[100]6NNCJ, (**e**) S[100]6NNCJ and (**f**) [110]6NNCJ.

with mechanism (b) 1NNNJ as they all result in a vacancy to migrate to its next-nearest-neighbour site. A similar comparison is also done between (c) 1TNNJ and (f) [100]6NNCJ. For six nearest-neighbour cyclic jumps (6NNCJ) mechanisms, a vacancy performs a cycle of six successive nearest-neighbour jumps (dashed lines with arrowhead) in such way that the initially perfect order is locally destroyed during the cycle but is totally restored upon its completion, except that the Ta vacancy migrates to its next-nearest-neighbour site along [100] direction for B[100]6NNCJ (figure 4d) and S[100]6NNCJ (figure 4e) or to its third-nearest-neighbour site along [110] direction for [110]6NNCJ (figure 4f). The terms bent and straight used here mean that the migrations of the vacancy and associated three atoms are in one plane and out one plane, respectively.

The migration energy is determined as follows: The vector of each jump is defined to connect the initial and final equilibrium positions of the vacancy. The atom exchanging with the vacancy is moved towards the vacancy along the negative jump vector. Each jump is achieved by a series of small steps. At each step the total energy of the simulation cell is minimized to the lowest value through full relaxation of the atoms. The maximum (saddle point) energy Q (that is activation energy of the diffusion) of the system minus the initial energy E_v^f (that is the formation energy of the defect at initial position) of the system is defined as the migration energy E_v^{m} of the defect. That is [27]

$$E_v^{\mathrm{m}} = Q - E_v^f. \tag{13}$$

3. Results and discussions

The determined lattice constant a, cohesion energy $E_{\rm c}$ and formation energy $\Delta E_{\rm c}$ of the alloy, and the cohesion energies of Ta, $E_{\rm c}({\rm Ta})$, and W, $E_{\rm c}({\rm W})$, in the alloy are listed in table 3 together with the available values of the *ab initio* calculations for comparison. The determined lattice constant a of 3.2316 Å and the formation energies $\Delta E_{\rm c}$ of -0.0950 eV for the alloy are in good agreement with the *ab initio* calculations of $a = 3.2450$ Å and $\Delta E_{\rm c} = -0.1035$ eV, respectively [13].

The calculated formation energies of vacancy E_v^f and anti-site defect $E_{\rm ant}^f$ are listed in table 4. It can be seen that the formation energies 0.9730 and -0.6583 eV for Ta and W anti-site defects are much lower than 3.4814 and 3.7014 eV, the formation energies for Ta and W vacancies. So we conclude that the anti-site defects are more favourable. This means that while the Ta component is slightly rich in TaW alloy, the abundant Ta atoms will occupy W sublattices to form Ta anti-site defects rather than the W vacancies. On the contrary, when the W component is slightly rich in the TaW alloy, the abundant W atoms will occupy Ta sublattices to form the W anti-site defects rather than the Ta vacancies.

Variation of the system energy with the displacement of vacancy moving along migration paths are shown in figure 5 for (a) 1NNJ, (b) 1NNNJ, (c) 1TNNJ, (d) B[100]6NNCJ, (e) S[100]6NNCJ and (f) [110]6NNCJ. The green lines with closed circles and blue lines with open circles correspond to $V_{\rm Ta}$ and $V_{\rm W}$, respectively. The vacancy displacements at each jump are normalized to a jump vector length of $(\sqrt{3}/2)a$ for (a) 1NNJ, (d) B[100]6NNCJ, (e) S[100]6NNCJ and (f) [110]6NNCJ, a for (b) 1NNNJ and $\sqrt{2}a$ for (c) 1TNNJ. We can see that, except (b) 1NNNJ and (c) 1TNNJ, the energy displacement curve is not symmetrical about the midpoint of each jump and the saddle point deviates from the midpoint towards either the initial or the final position of the migrating vacancy. This is because, while the migrating atom is assumed to be removed, the crystal structures constructed by the remaining atoms are not symmetrical about the midpoint of the jump vector. The activation energy Q (the maximum energy throughout all migration process) and the migration energy $E_v^{\rm m}$ are listed in table 5. We can see that, in six migration mechanisms of a Ta (or W) vacancy, the 1NNJ is the most favourable because of its lowest activation and migration energies. But such a migration, as can been seen in figure 4a, will result in a disorder in the ordered alloy (one anti-site plus one vacancy). To maintain

Table 3. Calculated lattice constant a, cohesion energy $E_{\rm c}$, formation energy $\Delta E_{\rm c}$ of the TaW alloy and the cohesion energy of Ta, $E_{\rm c}({\rm Ta})$, and W, $E_{\rm c}({\rm W})$ in the TaW alloy.

Method	a (Å)	$E_{\rm c}$ (eV)	$\Delta E_{\rm c}$ (eV)	$E_{\rm c}({\rm Ta})$ (eV)	$E_{\rm c}({\rm W})$ (eV)
MAEAM	3.2316	8.5950	-0.0950	8.6012	8.5888
Ab initio	3.2450 [13]		-0.1035 [13]		

Table 4. Calculated formation energies E_v^f (eV) for different point defects in TaW alloy.

Vacancy		Anti-site defect	
V_{Ta}	V_W	Ta_W	W_{Ta}
3.4814	3.7014	0.9730	−0.6583

the ordered property of the alloy and the required lower migration energy, the 1NNNJ or 1TNNJ can be achieved by six successive 1NNJ constructed here. For the 1NNNJ of a Ta (or W) vacancy, the S[100]6NNCJ (especially) and B[100]6NNCJ are preferred to 1NNNJ. Similarly, for the 1TNNJ of a Ta (or W) vacancy, the [110]6NNCJ is preferred to 1TNNJ. Furthermore, for each migration mechanism of the vacancy, the migration of a Ta vacancy is easier than that of a W vacancy.

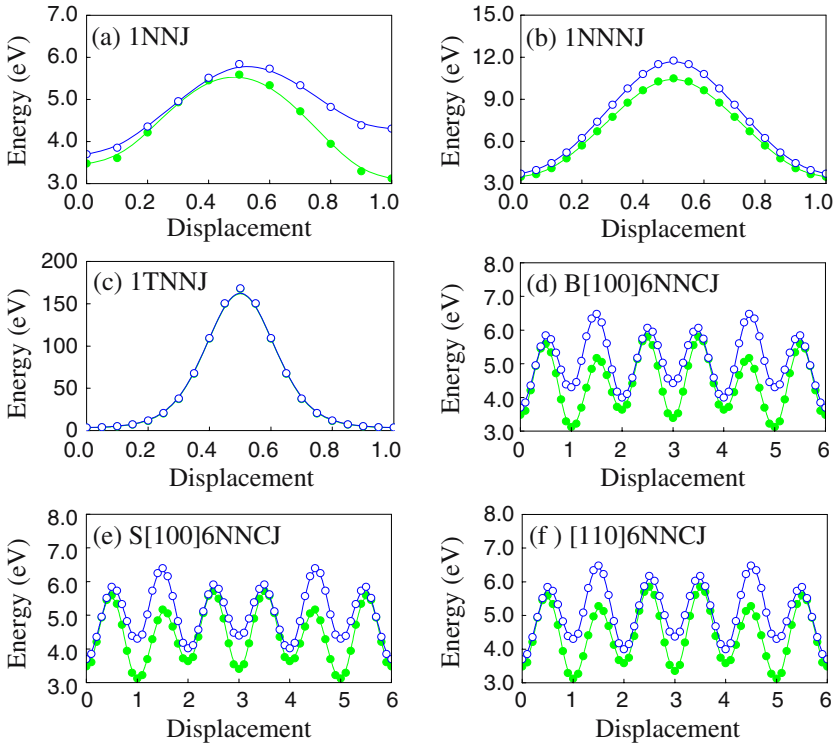

Figure 5. Energy displacement curves for (**a**) 1NNJ, (**b**) 1NNNJ, (**c**) 1TNNJ, (**d**) B[100]6NNCJ, (**e**) S[100]6NNCJ and (**f**) [110]6NNCJ of a Ta vacancy V_{Ta} (green lines with closed circles) and a W vacancy V_W (blue lines with open circles).

Table 5. The activation energy Q and migration energy E_v^m for 1NNJ, 1NNNJ, 1TNNJ, B[100]6NNCJ, S[100]6NNCJ and [110]6NNCJ of a Ta vacancy V_{Ta} or a W vacancy V_W in TaW alloy.

Vacancy	Energy (eV)	1NNJ	1NNNJ	1TNNJ	B[100]6NNCJ	S[100]6NNCJ	[110]6NNCJ
V_{Ta}	Q	5.5995	10.4985	167.4899	5.8178	5.7314	5.8598
	E_v^m	2.1181	7.0171	164.0085	2.3364	2.2500	2.3784
V_W	Q	5.8586	11.7561	168.1582	6.4899	6.4016	6.4899
	E_v^m	2.1572	8.0547	164.4568	2.7885	2.7002	2.7885

4. Conclusions

Combining molecular dynamics (MD) simulation with modified analytic embedded-atom method (MAEAM), the formation and migration behaviours of different point defects in B_2-type TaW ordered alloy have been investigated. The following conclusions are obtained:

1. The calculated lattice constant, 3.2316 Å and formation energy, -0.0950 eV for TaW ordered alloy are in good agreement with the *ab initio* data. The cohesion energies of the alloy, and the Ta and W components are 8.5950, 8.6012 and 8.5888 eV, respectively.
2. The anti-site defects $\mathrm{W_{Ta}}$ (especially) and $\mathrm{Ta_W}$ are easier to form than Ta and W vacancies. In other words, when the Ta (W) component is slightly rich in TaW alloy, the abundant Ta (W) atoms will occupy W (Ta) sublattices to form the $\mathrm{Ta_W}$ ($\mathrm{W_{Ta}}$) anti-site defects instead of W (Ta) vacancies.
3. Out of the six migration mechanisms of a Ta or W vacancy, the 1NNJ is the most favourable one because of its lowest activation and migration energies, but it will result in a disorder in the TaW ordered alloy.
4. To maintain the ordered property of the alloy as well as the lower migration energy, the 1NNNJ and 1TNNJ of a Ta or W vacancy can be achieved by S[100]6NNCJ (especially) or B[100]6NNCJ and [110]6NNCJ, respectively.

Acknowledgement

The authors would like to acknowledge the State Key Development for Basic Research of China (Grant No. 2004CB619302) for providing financial support for this research.

References

[1] Y J Liu, Y Ge, D Yu, T Y Pan and L J Zhang, *J. Alloy Compounds* **470**, 176 (2009)
[2] S Mrowec and Z Grzesik, *J. Phys. Chem. Solids* **65**, 1651 (2004)
[3] C Ratsch, A Zangwill, P Smilauer and D D Vedensky, *Phys. Rev. Lett.* **72**, 3194 (1994)
[4] M S Daw and M I Baskes, *Phys. Rev.* **B29**, 6443 (1984)
[5] M Menon, E Richter, A Mavrandonakis, G Froudakis and A N Andriotis, *Phys. Rev.* **B69**, 115322 (2004)
[6] V Blum and A Zunger, *Phys. Rev.* **B69**, 020103 (2004)
[7] Y C Ma, P O Lehtinen, A S Foster and R M Nieminen, *Phys. Rev.* **B72**, 085451 (2005)
[8] F C Zhang, Z Y Zhang, W H Zhang, J F Yan and J N Yun, *Chin. Phys. Lett.* **26**, 016105 (2009)
[9] Y J Cho, C H Kim, H S Kim, J Park, H C Choi, H J Shin, G H Gao and H S Kang, *Chem. Mater.* **21**, 136 (2009)
[10] B Baumeier, P Krüger and J Pollmann, *Phys. Rev.* **B76**, 085407 (2007)
[11] I J Wu and G Y Guo, *Phys. Rev.* **B76**, 035343 (2007)
[12] C Jiang, C Wolverton, Jorge Sofo, L Q Chen and Z K Liu, *Phys. Rev.* **B69**, 214202 (2004)
[13] C Bercegeay, G Jomard and S Bernard, *Phys. Rev.* **B77**, 104203 (2008)
[14] P E A Turchi, A Gonis, V Drchal and J Kudrnovský, *Phys. Rev.* **B64**, 085112 (2001)
[15] B W Zhang and Y F Ouyang, *Phys. Rev.* **B48**, 3022 (1993)

[16] B W Zhang, Y F Ouyang, S Z Liao and Z P Jin, *Physica* **B262**, 218 (1999)
[17] W Y Hu, B W Zhang, S Z Liao and B Y Huang, *J. Alloy Compounds* **287**, 159 (1999)
[18] Y Xie and J M Zhang, *Can. J. Phys.* **86**, 801 (2008)
[19] J M Zhang, X M Wei and H Xin, *Appl. Surf. Sci.* **243**, 1 (2005)
[20] J M Zhang, Y Yang, K W Xu and V Ji, *Can. J. Phys.* **86**, 935 (2008)
[21] J M Zhang, X L Song, X J Zhang, K W Xu and V Ji, *Surf. Sci.* **600**, 1277 (2006)
[22] J M Zhang, G X Chen and K W Xu, *Physica* **B390**, 320 (2007)
[23] G X Chen, J M Zhang and K W Xu, *J. Alloy Compounds* **430**, 102 (2007)
[24] H R Gong, L T Kong, W S Lai and B X Liu, *Phys. Rev.* **B66**, 104204 (2002)
[25] E A Brandes, *Smithells metals reference book*, 6th edn (Butterworths, London, 1983)
[26] R A Johnson, *Phys. Rev.* **B39**, 12554 (1989)
[27] M I Pascuet, R C Pasianot and A M Monti, *J. Mol. Catal.* **A167**, 165 (2001)